

Analysis of Electric Signals from Micro-Solid Oxide Fuel Cell Sensors Detecting Methane Biogas

Thitirat Ninwijit,^a Arkom Palamnit,^b Montri Luengchavanon,^{c,*} Sutida Marthosa,^d Nafisah Osman,^e Shahariar Chowdhury,^f and Sutham Niyomwas ^g

Micro-solid oxide fuel cells (SOFC) sensors prepared *via* depositing a thin film BYCF (10 wt% [Ba_{0.95}FeY_{0.05}O_{2.8}] + 90 wt% [Co₂O₃]) - GDC₂₀ (Gd_{0.20}Ce_{0.80}O_{1.95}) cathode and NiO-GDC₂₀ (Gd_{0.20}Ce_{0.80}O_{1.95}) anode on a GDC₂₀ electrolyte layer were operated at 800 °C. The structure, which receives only biogas, was formed into 15-mm pellets with only one side for detecting methane (CH₄). The detection of 40% to 99.99% CH₄ provided a high level of accuracy compared with 10% to 30% CH₄. The biogas (60% CH₄) from the Oil Palm Industry and Rubber Cooperative Fund, Thailand, increased remarkably at voltage levels of 20 to 21 mV. The electrical signal from the micro-SOFC sensor corresponded to the quantity of CH₄, with the chemical reaction of the dry reforming activities (NiO and Co₃O₄) highly catalyzed and transformed from CH₄ to H₂, thus generating electrons. It was concluded that the micro-SOFC sensor is suitable for detecting methane measurements at intermediate temperatures, with the ceramic structure offering low degradation compared with metal sensors.

DOI: 10.15376/biores.17.1.281-298

Keywords: Micro-SOFC; Catalyst; Sensor; Bio-Methane; Electrical signal; NiO; Co₃O₄

Contact information: a: Energy Technology program, Faculty of Engineering, Prince of Songkla University, Hat Yai, Songkhla 90110, Thailand; b: Faculty of Engineering, Prince of Songkla University, Hat Yai, Songkhla 90110, Thailand; c: Wind Energy and Energy Storage Systems Centre (WEESYC), Sustainable Energy Management Program, Faculty of Environmental Management, Prince of Songkla University, Hat Yai, Songkhla 90110, Thailand; d: Faculty of Science and Industrial Technology, Prince of Songkla University, Suratthani Campus, Surat Thani 84000, Thailand; e: Faculty of Applied Sciences, Universiti Teknologi MARA, Perlis Branch, 02600, Arau, Perlis, Malaysia; f: Faculty of Environmental Management, Prince of Songkla University, Hat Yai, Songkhla 90110, Thailand; g: Department of Mechanical Engineering, Faculty of Engineering, Prince of Songkla University, HatYai, Songkhla 90110, Thailand

* Corresponding Author: montri.su@psu.ac.th

INTRODUCTION

Solid oxide fuel cells (SOFCs) have attracted considerable attention due to their capacity to serve as a power source for supplying methane or biogas; both of these types of gas can be reformed to hydrogen gas (H₂) (Gür 2016). They are particularly well known for their high efficiency and fuel flexibility. Potentiometric measurements of synthesised ceramic composites were carried out to test an apparatus for hydrogen gas. These sensors act on the proton conductor element Sr₃CaZr_{0.9}Ta_{1.1}O_{8.55}, which indicates stable output potential close to the theoretical value calculated with the Nernst equation. The proton conductor elements of SrCe_{0.95}Yb_{0.05}O_{3- α} , CaZr_{0.9}In_{0.1}O_{3- α} , and Ba₃(Ca_{1.18}Nb_{1.82})O_{9- α} can be operated with a deviation over 100 mV between the theoretical and experimental data, which was obtained for sensing hydrogen gas (H₂) (Serret *et al.* 2011). Additionally, SOFCs are compatible with natural gas, propane, methanol, and ethanol (Kushi 2016). The

fabrication of 30 μm thin film $\text{Gd}_{0.2}\text{Ce}_{0.8}\text{O}_{2-\delta}$ (GDC) electrolyte using a screen-printing method has been shown to produce a maximum power density of 188 mW/cm^2 at 500 $^\circ\text{C}$ for a H_2 /air fuel cell (Xia *et al.* 2001). Therefore, the GDC materials can be deposited onto a thin film to provide the highest ionic conductivity, enabling the sensing SOFC to enhance the conduction of electrons from sensing H_2 gas. The SOFC sensors show a rapid response to H_2 gas streams ranging between 1 and 100 vol%. Additionally, the SOFC system generates the electricity by H_2 gas. SOFC sensors can also generate electricity by methane (CH_4) gas, which enhances catalytic for the dry reformation of CH_4 . The catalytic materials can reform the CH_4 to H_2 , such as nickel oxide and cobalt oxide (Ashok *et al.* 2019; Jadhav *et al.* 2016; Wei *et al.* 2018).

While chromatography systems are used in the majority of gas detectors (Cruz *et al.* 2015), flame ionization detectors (FID) have also been developed for gas chromatography (GC) based on gas detectors (Kim *et al.* 2019) and thermal conductivity (TCD) (Rastrello *et al.* 2013). Nevertheless, these detectors have several limitations. For instance, FID requires many types of carrier gases and TCD has low sensitivity to hydrocarbons and hydrogen gas, limiting their applications with GC. Nanomaterials based on semiconductor-detectors (Tian *et al.* 2013) and fuel cell technology (Lengden *et al.* 2013) have been designed with the ability to enhance the measurement sensitivity of chromatography systems, but with a simplified structure and size reduction. This design allows the detectors to overcome problems faced by conventional methods using GC, especially regarding the long-term stability and cross sensitivity of SOFC detectors deployed in a portable GC. Therefore, there is a need for an SOFC to be developed that can enable the electronic structure of the entire GC system to be analysed, with better detection limits than conventional FID and TCD methods and with fewer required chromatographic columns and types of carrier gases (Fan *et al.* 2017).

This work employed a novel design to investigate SOFCs in gas detectors under an intermediate temperature of 800 $^\circ\text{C}$. BYCF-GDC₂₀, GDC₂₀, and NiO-GDC₂₀ were selected as the cathode, electrolyte, and anode, respectively. A narrow space was located between the anode and the cathode using a triangular-saw tooth design. The Pt wires were current collectors that connected to the cathode and anode of the sensor for transmitting electrical signals. The electrical signal analysis in the SOFC sensor was analysed for CH_4 based on the chemical reaction and catalyst materials.

EXPERIMENTAL

Preparation of Cathode Composite

A cathode composite BYCF ($\text{Ba}_{0.054}\text{Y}_{0.029}\text{Co}_{1.8}\text{Fe}_{0.062}\text{O}_{2.89}$) (Hing *et al.* 2015; Suklueng *et al.* 2014) was prepared using reagent grade metal oxide powders from Sigma Aldrich, City, Germany. A mixture with a composition with 5 wt% BaO, 3 wt% Fe_2O_3 , 2 wt% Y_2O_3 , and 90 wt% Co_3O_4 was obtained in solid state with conventional ceramic powder processing (Fuel cell Materials, Ohio, USA).

Preparation of Electrolyte Composite

Commercial GDC₂₀ (20% gadolinium doped ceria, $\text{Gd}_{0.20}\text{Ce}_{0.80}\text{O}_{1.95}$) electrolyte powder was obtained from Fuel Cell Materials (Ohio, USA), with properties of a surface area of 10 to 14 m^2/g and particle size of 0.1-0.4 μm .

Preparation of Anode Composite

The NiO anode powder was also imported from Fuel Cell Materials USA (Columbus, Ohio, USA), with properties of a surface area of $2.9 \text{ m}^2/\text{g}$ and particle size of 0.5 to $1.5 \text{ }\mu\text{m}$. The cathode was a 50:50 mixture of BYCF and GDC₂₀, and the anode was a 60:40 mixture of NiO and GDC₂₀, respectively.

Preparation of Sensor

These compositions were used to control and maintain the thermal expansion coefficient (TEC) to be close to that of GDC₂₀, which is $13.08 \times 10^{-6} \text{ }^\circ\text{C}^{-1}$ at $900 \text{ }^\circ\text{C}$ (Guo *et al.* 2014). The electrolyte powder was ground for 1 h and then mixed with distilled water, including 10% polyvinyl alcohol (PVOH) (Mogul Carcare, Bangkok, Thailand) as binder, by weight (wt%). The cathode and anode composite was respectively milled for 12 h in a cylindrical capped container with alumina balls as filling using a horizontal rotary ball mill, and then dried in an oven at $150 \text{ }^\circ\text{C}$. The powders were ground again for 4 h in the authors' in-house-made grinding machine and sieved through a 150-mesh screen.

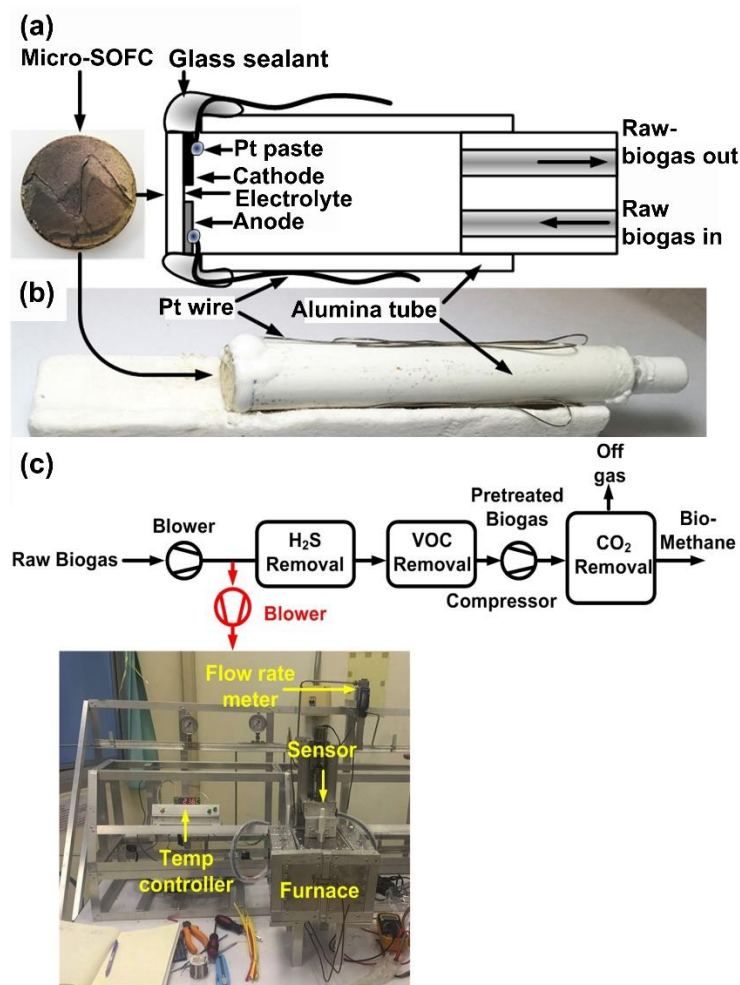


Fig. 1. Structure of micro-SOFC: (a) micro-SOFC exhibiting all the components for operational methane detection from biogas; (b) the micro-SOFC based on real experiments that was inserted in the furnace at $800 \text{ }^\circ\text{C}$ for sensing operations; (c) the plant layout for raw-biogas cleaning and upgrading as well as micro-SOFC sensor testing station can installation

The production of the micro-SOFC sensor started with the manufacture of the full fuel cell with a 50:50 BYCF + GDC₂₀ cathode and 60:40 NiO + GDC₂₀ anode deposited on the GDC₂₀ electrolyte pellet (50:50 BYCF + GDC₂₀|60:40 NiO + GDC₂₀| GDC₂₀). The GDC₂₀ powder was pressed to form a 15-mm diameter pellet of 2 mm thickness by uniaxial press under 3000 psi pressure. The GDC₂₀ pellet was sintered at 1,400 °C with a heating rate of 10 °C/min for 10 h under atmospheric pressure conditions (101.3 kPa). The 50:50 BYCF + GDC₂₀ cathode was deposited on the GDC₂₀ electrolyte pellet by spray pyrolysis (model; Ultra spray pyrolysis, Beijing, China) in which the triangular saw-tooth shape sticker covered the surface to control the shape of the cathode layer.

In the spray pyrolysis technique, the spray gun was operated at 120 psi air pressure, and the nozzle was set up at a height of 20 cm with a 16-cm spraying diameter. The pellet was placed on a stainless steel substrate and the temperature was increased to 450 °C. To use this technique, the cathode and anode mixtures had to be in the form of slurries; the mixtures were mixed with distilled water in the ratio 30:70 vol%, respectively. All slurries were milled for 12 h in a horizontal rotary ball mill for acquiring highly homogenous slurries.

After spraying the cathode, this pellet was co-sintered at 1,100 °C with a heating rate of 10 °C/min for 10 h under atmospheric pressure conditions. Meanwhile a 60:40 NiO + GDC₂₀ anode was also deposited on the GDC₂₀ electrolyte pellet, opposite to the cathode area, by spray pyrolysis in which the triangular saw-tooth shape sticker covered the cathode layer to control the shape of the anode and provided a space between the anode and cathode area. To obtain high porosity for the adsorption of gas and increase the electrochemical power density (Ohimain and Izah 2017), this pellet was co-sintered at 1,100 °C with a heating rate of 10 °C/min for 10 h under atmospheric pressure. The finished system is shown Fig. 1(a).

Figure 1(a) shows platinum electrodes as probes that were primed with a platinum paste and pressed to ensure good contact was made. The pellets with the platinum probes were placed in an in-house designed furnace. In the real experiment as shown in Fig. 1(b), the micro-SOFC employed biogas that inserted in the furnace at 800 °C for the sensing operation. Fig. 1(c) shows the plant layout for raw-biogas cleaning and upgrading. The plant has been separated into a cleaning section and an upgrading section. The cleaning section aims to migrate secondary components such as sulfur compounds (H₂S) and non-methane volatile organic compounds (VOC). An estimate of bio-methane quality has been operated to assess compliance with recent National and European standard specifications (Paolini *et al.* 2019). The micro-SOFC sensor can be installed by connecting a pipe and using the blower to control the flow rate of the raw-biogas to the micro-SOFC sensor testing station at a temperature of 800 °C.

Analytical Procedures

The DC electrical conductivity was measured using four point probes with varied temperatures at 25, 100, 200, 300, 400, 500, 600, 700, and 800 °C (Mitsubishi Chemical Analytech, Laresta-GX, MCP-T700, Tokyo, Japan). The surface area, pore volume, and pore size were measured using BET Micromeritics/ASAP2060 (Micromeritics, Norcross, USA). Microstructures were observed using a scanning electron microscope, field emission (FE)-SEM (Scios DualBeam, Prague, Czechia), and ZEISS (ZEISS Microscopy, Jena, Germany). The thermal expansion coefficients of all the sintered materials were determined using a Thermo Mechanical Analyser (TMA) from Setaram, France. The crystalline nature and phase purity were examined using powder X-ray diffraction (XRD) techniques

(PANalytical, Empyrean, United Kingdom) with Cu $K\alpha$ radiation. The voltage level for detecting quantities of methane in biogas was measured by digital multimeter (V&A, VA18B version, Shanghai, China). The biogas composition (H_2 , CO_2 , CH_4 , N_2 , and H_2S) was determined by using gas chromatography with a flame thermal conductivity and flame photometric detector by Agilent GC7890 (Agilent Technology, California, USA). Several ratios between 99.99% methane (CH_4) and 99.99% Nitrogen (N_2) gas were used to prepare different methane gas concentrations. The pressure was kept constant at 60 psi or around 0.5 L/min (Chea *et al.* 2020) and gases were mixed using metering valves from Swagelok (Cleveland, OH, USA). The biogas was collected from a palm oil factory (Chumphon) and rubber cooperative fund in the (Songkhla) south of Thailand.

RESULTS AND DISCUSSION

The composition of the 40:60 NiO + GDC₂₀ anode exhibited high porosity GDC₂₀ and was connected as a scaffold to enhance NiO dispersion due to its high surface area and porosity that can support the adsorption of the CH_4 gas. However, it is not easy to distinguish the separate particles of the NiO and GDC₂₀ phases due to lower GDC₂₀ amounts. Therefore, most of the morphology is produced from NiO phases. After reduction in hydrogen or reformed gas from CH_4 , the porosity of composites is increased, leading to a reduction in the NiO's surface (Jadhav *et al.* 2016; Maling *et al.* 2020). The pin holes that appeared between the grain of NiO and GDC₂₀ were around 1 μm , which resulted from the sintering at 1100 °C for 10 h and the spray pyrolysis technique, as shown in Fig. 2(a). The micrographs of the top-view of the cathode side that used the composition of the 50:50 BYCF + GDC₂₀ cathode also revealed high porosity with pin holes approximately 10 μm .

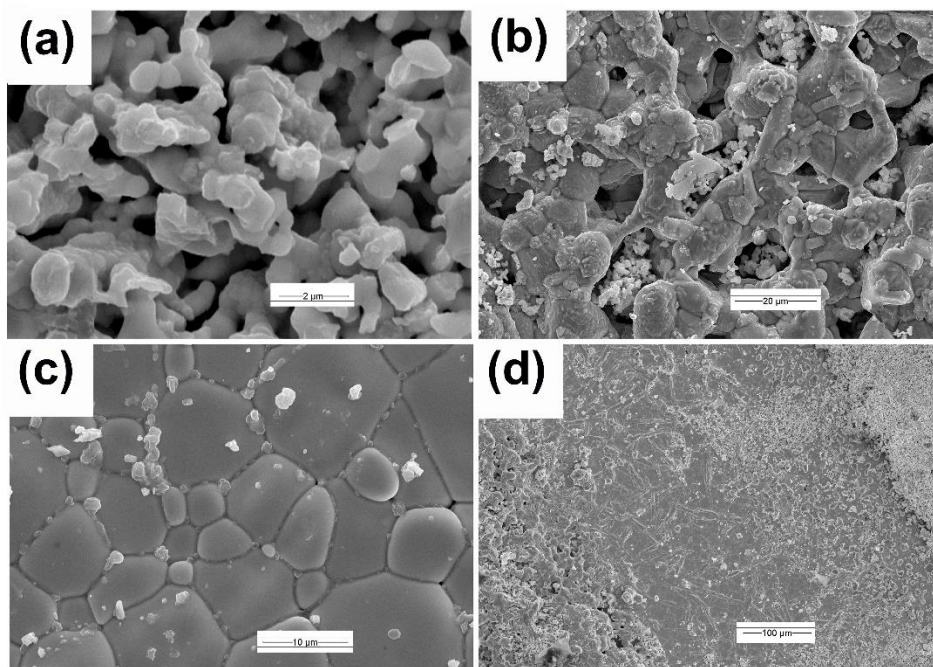


Fig. 2. SEM micrographs of micro-SOFCs based on the surface: (a) 60:40 NiO + GDC₂₀ anode, (b) 50:50 BYCF + GDC₂₀ cathode, (c) GDC₂₀ electrolyte, and (d) GDC₂₀ electrolyte located at the space between the anode and cathode

Figure 2(b) shows that the GDC₂₀ particles in cathode were in range of 0.1 to 0.4 μm, and Fig. 2(c) shows a dense electrolyte microstructure with minimal pores that was sintered at 1,400 °C for 10 h. The free-space was prepared between the cathode and anode surfaces. The space prevented the electrical signal short circuit from the conducting of cathode and anode, as shown in Fig. 2(d).

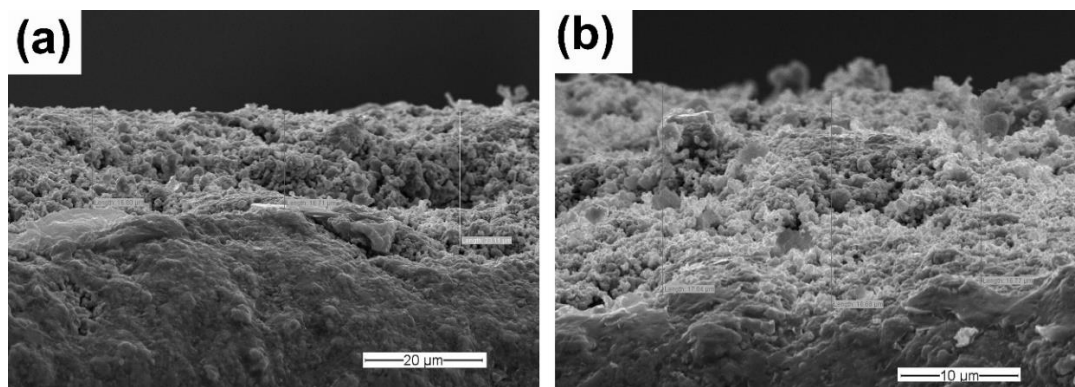


Fig. 3. Cross-section of micro-SOFC: (a) 40:60 NiO + GDC₂₀ anode deposited on electrolyte and (b) 50:50 BYCF+GDC₂₀ cathode deposited on GDC₂₀ electrolyte

Figure 3(a) shows a cross-sectional view of the 40:60 NiO + GDC₂₀ anode deposited on electrolyte at around 18.87 μm, and Fig. 3(b) shows the cross-sectional view of the 50:50 BYCF + GDC₂₀ cathode deposited on GDC₂₀ electrolyte at approximately 24.77 μm. These thicknesses were measured by the SEM machine (Table 1). The rough surface of the GDC₂₀ electrolyte may result from the compaction and the spray pyrolysis technique.

GDC₂₀ electrolyte is regarded as one of the more promising materials for low-intermediate temperature SOFCs. Because SOFCs need to have high density, the properties of Gd³⁺ and Ce⁴⁺ show a higher ionic radius that can react with excess oxygen vacancies, leading to higher ionic conductivity than pure ceria (Medisetti *et al.* 2017). The CeO₂ is a compound in GDC₂₀ that is based on ionic conductivity; the migration energy (E_M) is the energy required at the saddle point for O²⁻ to diffuse to the adjacent site; the migration energy is the activation energy for conductivity. E_M can be generated from the relationship shown in Eq. 1,

$$(f_{max})_h \propto \exp(-E_M/k_B T), \quad (1)$$

where $(f_{max})_h$ is temperature for the high-frequency, E_M is migration energy (eV), k_B is the Boltzman's constant, and T is the absolute temperature (K).

At operating temperatures above 800 °C, involving high-temperature SOFCs, the migration energy is the activation energy for conductivity. Additionally, at the intermediated-temperature (IT) SOFCs around 500 °C, the oxygen vacancies must be acquired from the trapping centers. E_O can be obtained from the relationship, $T[(\tan\delta)_{max}]_h = \exp(-E_O/k_B T)$. The isolation energy is the energy required for the captured O₂ vacancy to move freely (Lee *et al.* 2017). Equation 2 are as follows,

$$T[(\tan\delta)_{max}]_h = \exp(-E_O/k_B T) \quad (2)$$

where $\tan\delta$ is the loss tangent proportional to the loss factor, and E_O is dissociation energy (eV).

Table 1. Thickness of 50:50 BYCF + GDC₂₀ Cathode and 60:40 NiO + GDC₂₀ Anode Layers Deposited on GDC₂₀ Electrolyte

Micro-SOFC	Compositions	Thickness (μm)	Average Thickness (μm)	Standard Deviation
Cathode	50:50 BYCF + GDC ₂₀	25.50	24.77	± 0.675
		24.17		
		24.63		
Anode	60:40 NiO + GDC ₂₀	16.80	18.87	±3.669
		16.71		
		23.11		

Figure 4 depicts the XRD patterns of 50:50 BYCF + GDC₂₀ cathode powder obtained upon calcination at 1100 °C for 10 h. These peaks represented the BYCF and GDC₂₀ components that were combined at a high temperature. The phase of Ce_{3.568}Gd_{0.792}Y_{0.012} composition contributed GDC₂₀ doped with Y (Yttrium) from the BYCF compound. This composition when formed in solid solution will be helpful for increasing the sintering temperature of the composite cathode (Rehman *et al.* 2016, 2017). The phases of the BaFeO_{2.9} and Ba₃Co₂Fe₂₄O₄₁ compositions were represented from BYCF with a majority of Co₃O₄ leading to high conductivity and ionic transfer (Suklueng *et al.* 2014).

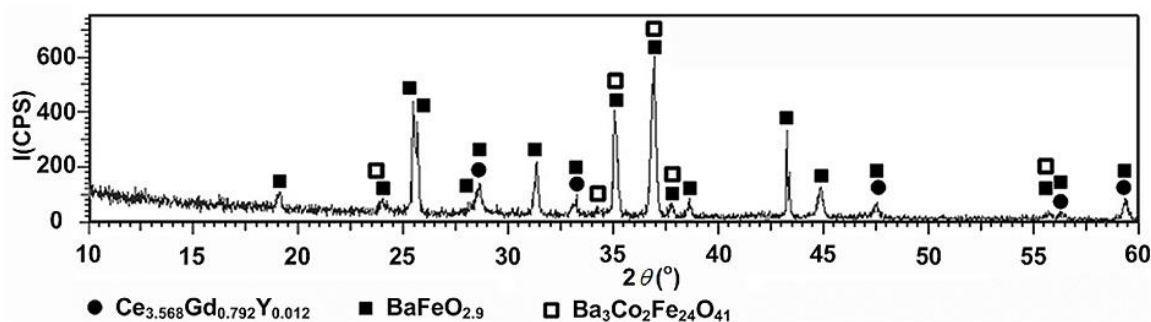
**Fig. 4.** XRD patterns of calcined 50:50 BYCF + GDC₂₀ cathode powder

Figure 5 shows the XRD patterns of GDC₂₀ electrolyte power obtained through calcination at 1400 °C for 10 h. The major peak was formed with CeO₂O₃ and Gd₂O₃, which generated some Ce⁴⁺ in the CeO₂ structure by Gd³⁺; this is a promising candidate for low operational temperatures, producing relatively high ionic conductivities and well known among ceria-based on materials solid electrolyte (Choolaei *et al.* 2018). The GDC₁₀ electrolyte was operated in a micro-SOFC methane sensor that showed high ionic conductivity for generating an electric signal (Phaijit *et al.* 2019). The GDC₂₀ compound was formed in nanofibers that can be activated for high electrical conductivity at more than 0.01 S/cm above 600 °C (Thiabdokmai *et al.* 2014). The nanocrystalline thin film CeO₂ sensor was operated to monitor oxygen. Temperature was used in a range from 700 to 750 °C. These conditions appeared to be excellent for sensor operation, leading to a fast reaction to the exchange of O₂ concentration that can be represented in the resistance range (Jasinski *et al.* 2003). Figure 6 depicts the XRD patterns of 60:40 NiO + GDC₂₀ anode powder obtained by calcination at 1100 °C for 10 h. These peaks revealed NiO, Ce_{0.8}Gd_{0.2}O₂, and CeO₂, whose phases separated using high temperatures under calcination. NiO made up most of the phase leading to the high quantity while the minority of the phase was

$\text{Ce}_{0.8}\text{Gd}_{0.2}\text{O}_2$ and CeO_2 . NiO acts as an excellent catalyst for oxygen activation, while producing high electrical conductivity with GDC_{20} and mainly reacting as a matrix to support the catalyst and prohibit the Ni element from agglomeration with operating conditions (Ding *et al.* 2009; Hajakbari *et al.* 2020).

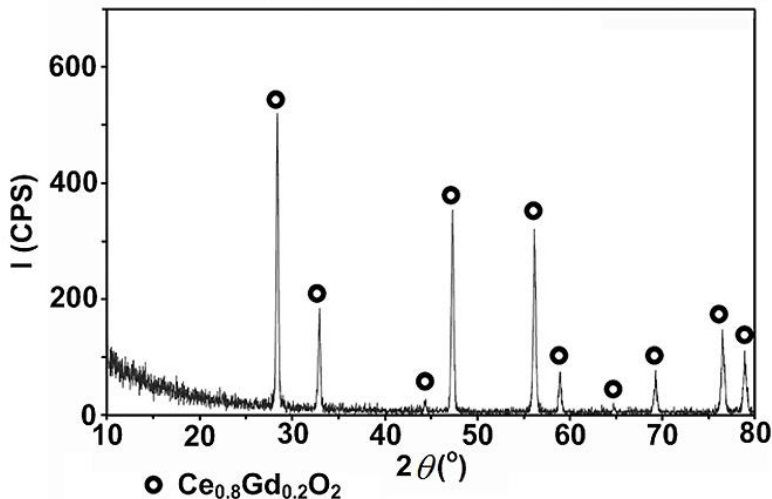


Fig. 5. XRD patterns of calcined GDC_{20} electrolyte powder

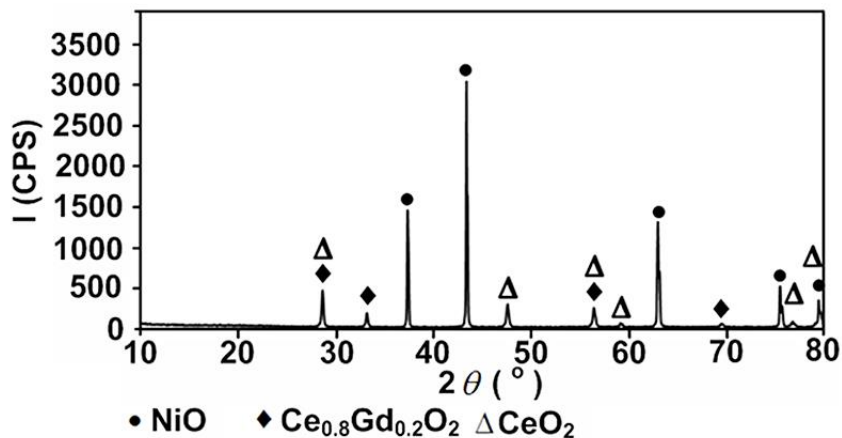


Fig. 6. XRD patterns of calcined 60:40 NiO + GDC_{20} anode powder

Table 2 shows the thermal expansion comparison between the 50 wt% BYCF + 50 wt% GDC_{20} cathode, GDC_{20} electrolyte, and 60 wt% NiO + 40wt% GDC_{20} anode in the temperature ranges of 40 to 200 °C, 40 to 400 °C, 40 to 600 °C, and 40 to 800 °C. Generally, the total expansion values obtained for GDC_{20} were $12 \times 10^{-6}/\text{°C}$ (Setevich *et al.* 2012) and for the BYCF composition $12.79 \times 10^{-6}/\text{°C}$ (Suklueng *et al.* 2014). Optimization of thermal expansion was achieved with a mixture of GDC_{20} to BYCF and NiO as the cathode and anode components. The best results were obtained at $12.95 \times 10^{-6}/\text{°C}$ at 40 to 800 °C. Therefore, these TECs can be used for micro-SOFC.

Table 2. Thermal Expansion Coefficients for 50 wt% BYCF + 50 wt% GDC₂₀ Cathode, GDC₂₀ Electrolyte, and 60 wt% NiO + 40 wt% GDC₂₀ Anode

Compositions	Temperature (C°)			
	40 to 200	40 to 400	40 to 600	40 to 800
	TEC (10 ⁻⁶ /°C)			
50 wt% BYCF + 50 wt% GDC ₂₀	10.89	10.80	10.46	12.34
GDC ₂₀	10.73	10.91	11.47	12.95
60wt% NiO + 40wt% GDC ₂₀	10.37	11.88	11.38	11.84

Table 3 shows the properties (surface area, pore volume, and pore size) of the generated micro-SOFC cathode, electrolyte, and anode. The properties of the GDC₂₀ electrolyte required the lowest surface area, pore volume, and pore size, because the GDC₂₀ is the electrolyte that needs high density for ionic conductivity. The nano-particle of GDC₂₀ was sintered at 500 °C, which fabricated surface area of 13.2 m²/g (Muñoz *et al.* 2015). The GDC₂₀ sintered at high temperature can generate high density and low surface area. In addition, the properties of the cathode and anode require a high surface area, pore volume, and pore size because it increases the possibility for the gas to the chemical reaction (Araujo *et al.* 2018). However, the surface area, pore volume, and pore size were related in the SEM micrographs in Fig. 2(a) to (c).

Table 3. Comparison of the Properties of Micro-SOFC Components Using the BET Machine

Micro-SOFC Components	Compositions (wt%)	BET Surface Area (m ² /g)	Pore Volume (cm ³ /g)	Pore size (Å)
Cathode	50 wt% BYCF + 50 wt%GDC ₂₀	1.3506	0.002752	8.151520
Electrolyte	GDC ₂₀	0.1401	0.000050	1.439490
Anode	60 wt% NiO +40 wt% GDC ₂₀	1.0783	0.021154	784.7491

Figure 7(a) shows the resistivity of the 60 wt% NiO + 40 wt %GDC₂₀ anode in temperatures ranging from 40 to 800 °C. At high temperatures (500 to 800 °C), 60 wt% NiO + 40 wt% GDC₂₀ clearly show low resistivity. The 60 wt% NiO composition was predominantly electronic (typical of metals), while the 40 wt% composition was rare earth GDC₂₀ with a major component of CeO₂, providing high ionic conductivity. Therefore, the cermet conductivity occurs through two mechanisms: ionic (through the GDC phase) and electronic (through the metallic nickel phase) (Santos *et al.* 2018). This anode composition generated an average *E_a* of 0.13 eV. The lower activation energy (less than 1 eV) indicated that NiO contributed greatly to the electronic conductivity. Figure 7(b) shows the resistivity of the 50 wt% BYCF + 50 wt% GDC₂₀ cathode in various temperatures ranging from 40 to 800 °C. Suklueng reported that BYCF indicated high electrical conductivity of 588.55 S cm⁻¹ at 800 °C (Suklueng *et al.* 2014). Therefore, 50 wt% BYCF + 50 wt% GDC₂₀ composites can decrease conductivity with the properties of GDC₂₀ but improve ionic transfer and thermal expansion (Table 2).

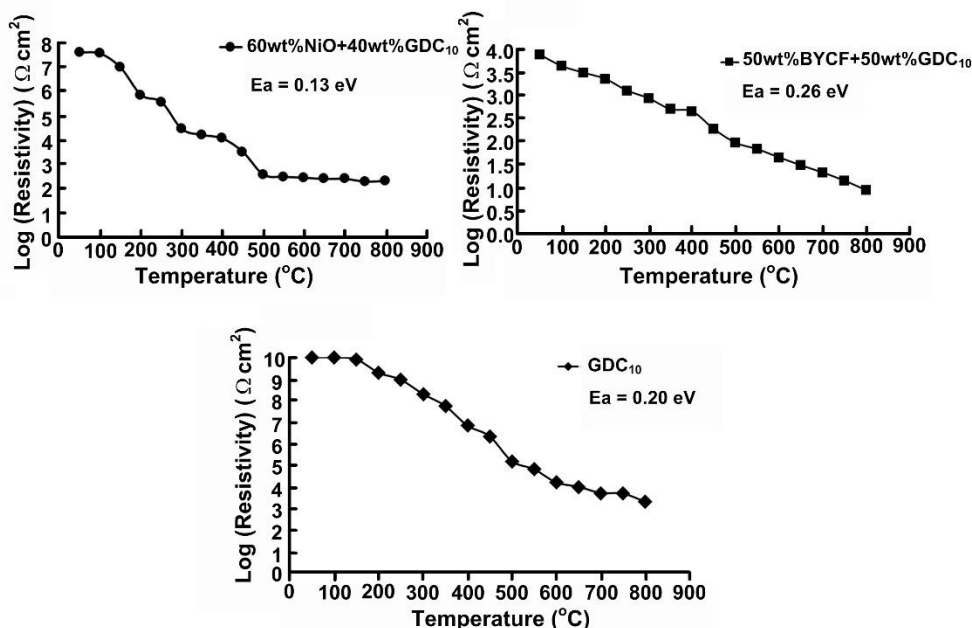


Fig. 7. Variations of the resistivity with temperature for the (a) 60 wt% NiO + 40 wt% GDC₂₀ anode, (b) 50 wt% BYCF + 50 wt% GDC₂₀ cathode, and (c) GDC₂₀ electrolyte composite in the range $40 \leq T \leq 800$ °C, under atmospheric air conditions

While BYCF exhibited an E_a of around 3.23 eV, 50 wt% BYCF + 50 wt% GDC₂₀ can generate 0.26 eV at 800 °C, which indicates the addition of 50 wt% GDC₂₀ to develop for best cathode materials. Figure 7(c) shows the resistivity of the GDC₂₀ electrolyte at starting temperature of 40 °C up to 800 °C. This resistivity was higher than values for the 60 wt% NiO + 40 wt% GDC₂₀ anode and the 50 wt% BYCF + 50 wt% GDC₂₀ cathode. The high resistivity material prevents the short circuits in the micro-SOFC and the E_a of GDC₂₀ measuring 0.20 eV at 800 °C. Kulkarni *et al.* (2014) and Sui *et al.* (Liu *et al.* 2013) reported conductivities of 0.97×10^{-2} and 1.40×10^{-2} S cm⁻¹ at 700 °C, respectively. Based on GDC₂₀, this compound exhibited mixed ionic and electronic cathode and anode, which can be attributed to the promotion of electron conductivity (N-type) in a reducing atmosphere and electron hole conductivity (P-type) in an oxidizing atmosphere (Niaz *et al.* 2019).

Table 4. Biogas Compositions Collected from the Oil Palm Industry at Chumphon, Thailand

Biogas From Oil Palm Industry at Chumphon, Thailand	Compositions of Biogas (%Volume)				
	H ₂	N ₂	CH ₄	CO ₂	H ₂ S (ppm)
1 st Measurement	0.000	5.286	61.072	35.333	923.893
2 nd Measurement	0.000	4.921	60.592	34.781	953.304
3 rd Measurement	0.000	4.793	58.336	34.886	956.115
Average	0.000	5.000	60.000	35.000	944.437
Standard Deviation	0.000	0.256	1.461	0.293	17.847

This biogas contained N₂, CH₄, CO₂, and H₂S with values averaging (% Volume) 5 ± 0.256 , 60 ± 1.461 , 35 ± 0.293 , and 944.437 ± 17.847 (ppm), respectively. The methane (CH₄) was most of the biogas, while nitrogen (N₂), and carbon dioxide (CO₂) were the minority as shown in Table 4. Typical biogas compositions from the palm oil mill have also contained N₂, CH₄, CO₂, and H₂S with values between 0 to 1%, 55 to 75%, 30 to 45%, and 1 to 2%, respectively (Ohimain *et al.* 2017).

Table 5. Biogas Composition Collected from the Rubber Cooperative Fund at Songkhla, Thailand

Biogas From Rubber Cooperative Fund at Songkhla, Thailand	Compositions of Biogas (%Volume)				
	H ₂	N ₂	CH ₄	CO ₂	H ₂ S (ppm)
1 st Measurement	0.000	3.727	57.972	38.798	-
2 nd Measurement	0.000	6.605	58.769	34.944	-
3 rd Measurement	0.000	8.555	58.263	33.182	-
Average	0.000	6.296	58.334	35.641	-
Standard Deviation	0.000	2.429	0.403	2.872	-

This biogas contained N₂, CH₄, CO₂, and without H₂S, with values averaging (% Volume) 6.296 ± 2.429 , 58.334 ± 0.403 , and 35.641 ± 2.872 , respectively. The CH₄ was the majority of the biogas again, while N₂, and CO₂ were the minority, as shown in Table 5. Typical biogas compositions from the Rubber Cooperative Fund (rubber latex) have contained CH₄ and H₂S with values of $79.8 \pm 2.5\%$ and 6395 ± 2309 ppm, respectively (Charnnok *et al.* 2013). However, the processes of biogas productivity in the rubber latex industry are highly sensitive depending on the hydraulic retention time and organic loading rate (Chaiapat *et al.* 2015).

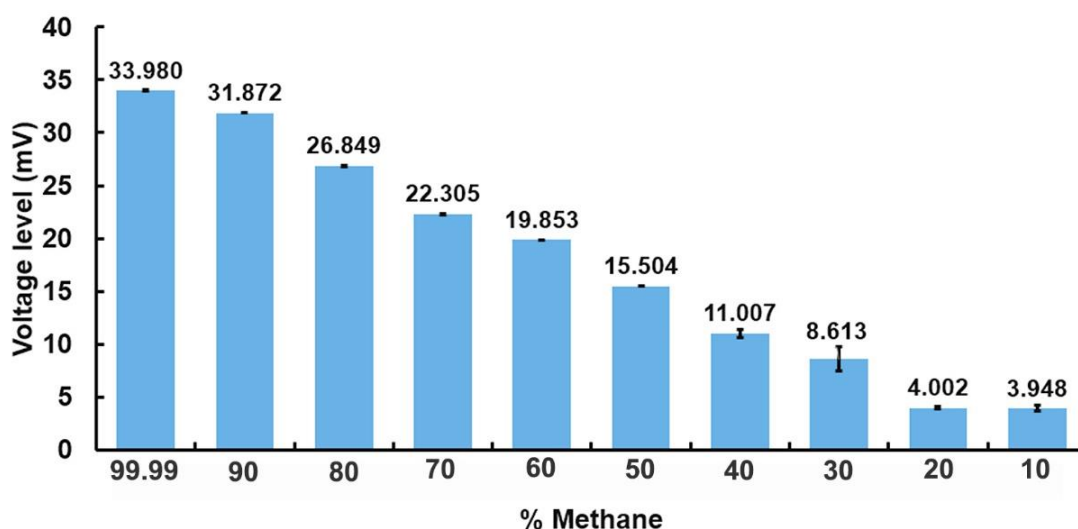
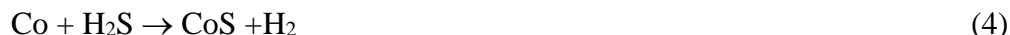


Fig. 8. The voltage level with varied percentages of methane (mixture gas) measured by the micro-sensor SOFC

Figure 8 shows the mixture gas containing methane gas (CH₄) and nitrogen gas (N₂), mixed at ratio from 10% to 99.99%. The micro-SOFC sensor was used for detection at voltage level of 33.980 mV (99.99% methane) with low error bar. The voltage level continuously decreased depending on the percentage of methane. The voltage level affected the intensity of the methane gas with high accuracy until 30 to 40% methane gas indicated a high error, while 10 to 20% methane showed that the voltage level did not affect the quantity of methane. Therefore, 50 to 99.99% methane was highly efficient for detecting due to generating numerous electrons. The quantity of 10 to 40% methane was insufficient to generate electrons in the micro-SOFC sensor, which can be explained by coking resistance catalyst for CO₂ dry reforming of CH₄. The anode side contained NiO that performed the high catalytic activity and resistance to carbon deposition following Equation 3 (Wei *et al.* 2018), which changed the CH₄ to H₂ based on the low methane affecting to NiO that could not act upon the endothermic nature of the CH₄ decomposition reaction for generating electrons in the micro-SOFC sensor. The related equations are as follows:



Generally, the biogas contained approximately 60% CH₄, depending upon materials and time duration (Chen *et al.* 2020). The biogas from the oil palm industry revealed a higher voltage level average of 20.90 mV, while biogas from the Rubber Cooperative Fund showed an average of 20.35 mV; and the mixture gas showed an average of 18.93 mV, as shown in Fig 9.

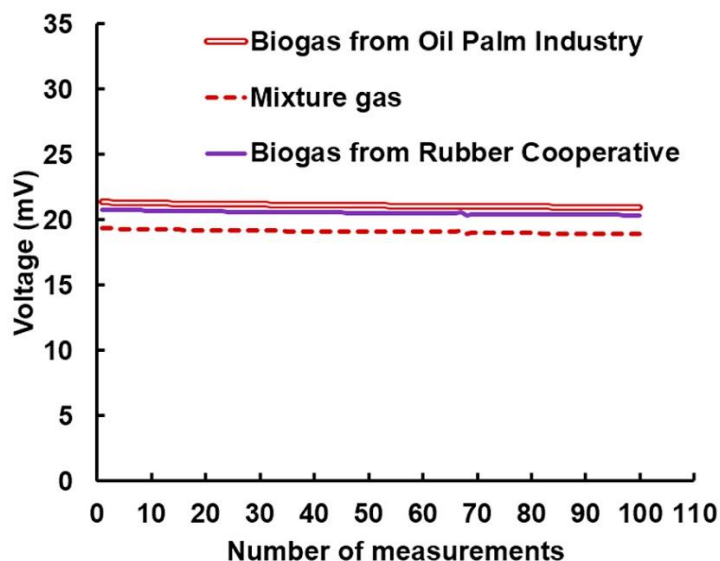


Fig. 9. Comparison of voltage levels between mixture gas (60%CH₄:40%N₂), biogas from the Rubber Cooperative Fund at Songkhla, and biogas from the oil palm industry at Chumphon, (Thailand) as measured by a micro-SOFC sensor

For the comparison of the quantity of biogas between Tables 4 and 5, the CH₄ from the oil palm industry was a little higher than for the Rubber Cooperative Fund; however, the CO₂ in both places had almost the same value. Meanwhile the biogas from the oil palm industry contained reduced amounts of H₂S. The micro-SOFC sensor can generate higher electron form the biogas from the oil palm industry affected by the CO₂ dry reforming of CH₄. The quantity of electrons for the signal in the micro-SOFC sensor was dependent on the quantity of CH₄ reacting with CO₂ that provided an enthalpy change of 247 kJmol⁻¹ at 298 K (Wei *et al.* 2018). The low voltage level of the mixture gas may be affected by the low CO₂ level when the mixture gas injected for measurement in the micro-SOFC sensor was only combined with the air in the alumina chamber.

Figure 10 shows the catalytic activity for reforming CH₄ to be H₂ gas and the generation of electrons formed in the micro-SOFC sensor. Focusing on the endothermic nature of CH₄ gas for the decomposition reaction at 700 °C, CO₂ is obtained by dry reforming of CH₄. The active-site mechanism has been popularly accepted for CO₂ reforming of CH₄ using Ni catalysts (Amin *et al.* 2017), where the C and H₂ could be decomposed from CH₄ on the Ni particles. According to this decomposition, the dissociation and adsorption of CH₄ on the Ni particles and of CO₂ on the substrate are properly the controlling factors for the reactions in the CO₂ dry reforming of CH₄. The H atoms in CH₄ are continuously released one-by-one, until the carbon is finally left on the surface of the Ni particles that are related to the higher surface area of 1.0783 m²/g in Table 3. For this reason, the deactivation of catalysts depends on the rate of carbon removal and formation (Pan *et al.* 2008).

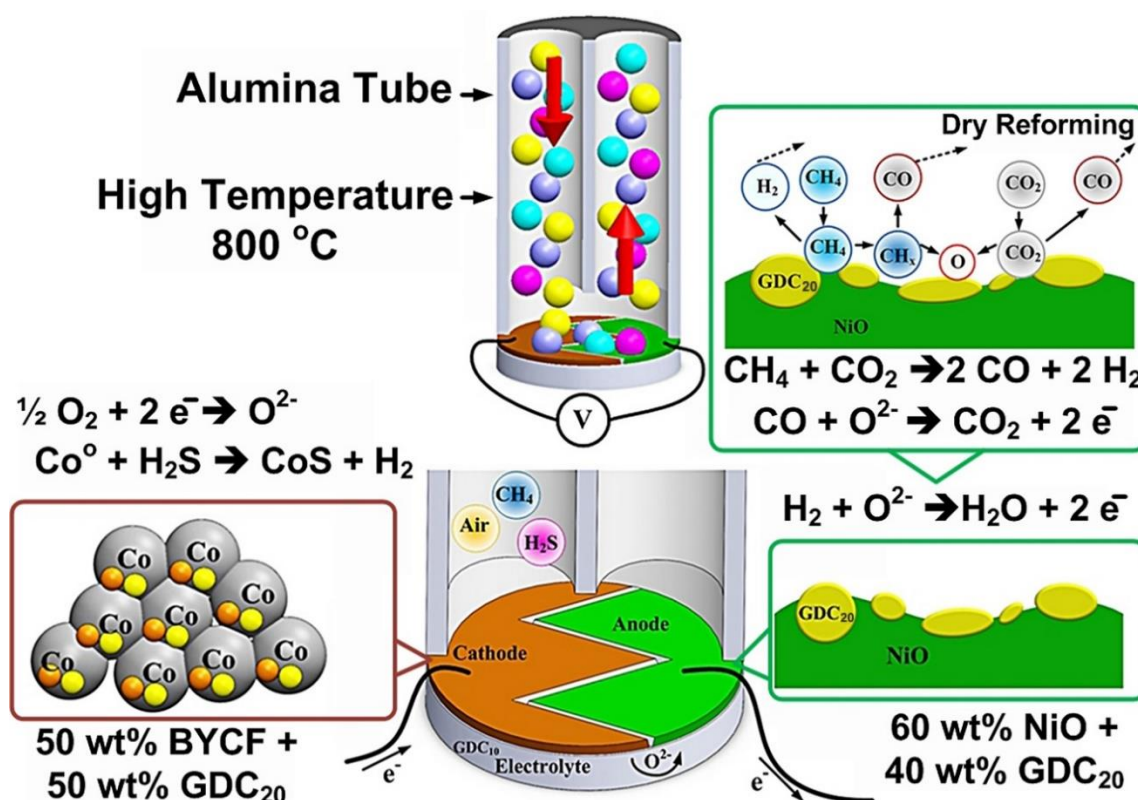


Fig. 10. Schematic mechanism for biogas dry reforming of CH₄ combined with principle of SOFC to be a micro-SOFC sensor

After the dry reforming activity, the micro-SOFC sensor produced the H₂. In the cathode side, oxygen ions are the reacted form of oxygen ($1/2 \text{O}_2 + 2\text{e}^- \rightarrow \text{O}^{2-}$), and then conducted through the electrolyte layer to the anode that crossed the air gap. Cobalt was also contained in the cathode side; they can perform the toluene reforming activity, which is primarily due to the C-C bond activity by metallic cobalt species. Deactivation can cause the encapsulation of active metal species by carbon and/or oxidation of metallic cobalt by oxide or sulfide species. The deactivation trend in the presence of sulfur compound is mainly due to the procession of inert cobalt sulfide compounds. The activity of cobalt-based catalysts in the formation of sulfur-containing feed primarily depends on the invariability of the formed cobalt sulfide compounds during the dry reforming reaction environment (Ashok *et al.* 2019). In this work, around 944.437 ppm H₂S as exhibited in Table 4 may split the H₂S to be H₂ for generating electrons. Even the reforming of CH₄ itself occurs, and the electron flow through the external electric for the micro-SOFC sensor (Phaijit *et al.* 2019). Moreover, in this gas reaction, the Gibbs free energy of the overall oxidation reaction of fuel ($\text{H}_2 + 1/2\text{O}_2 \rightarrow \text{H}_2\text{O}$, $\text{CO} + 1/2\text{O}_2 \rightarrow \text{CO}_2$) is also transformed into an electric signal, and the irreversible part is liberated as heat (Bao *et al.* 2018).

CONCLUSIONS

1. The micro-SOFC sensor was adapted from a normal SOFC power source to be a sensor for detecting CH₄. The novel design used a cathode and anode that were deposited on the electrolyte pellet. This micro-SOFC sensor operated at a high temperatures of 800 °C. The electrical signal of the micro-SOFC sensor is dependent on the quantity of CH₄ and can be applied as a means of detection.
2. The micro-SOFC sensor was first calibrated electrical signal with known concentration of synthetic methane gas, for example, 60% synthetic methane gas is prepared from mixing 60% of pure CH₄ and 40% of pure N₂. The average electrical signals received from feeding the 60% synthetic methane gas, the biogas from oil palm industry and the biogas from the Rubber Cooperative Fund were 18.93 mV, 20.90 mV, and 20.35 mV, respectively. The electrical signals were similar and reflected the actual biogas concentration tested by using GC.
3. The biogas generated a higher electric signal than (CH₄ + N₂) mixture gas, which was affected by the dry reforming reaction from CO₂. The dry reforming reaction, dissociation, and adsorption act upon the CH₄ while the Ni particles on anode side of the micro-SOFC sensor and the CO₂ on the substrate are properly the controlling factors for the reactions to reproduce H₂.
4. This micro-SOFC sensor was a novel design based on the structure of the SOFC, and can be operated at a high temperature of 800 °C. The micro-SOFC sensor methane part is low cost, but the operational system is costly due to the high temperature and the need for a furnace. Therefore, this sensor is suitable for measuring raw biogas with high temperature and without degradation due to the use of ceramic materials.

ACKNOWLEDGMENTS

This research was supported financially by the Wind Energy and Energy Storage Systems Centre (WEESYC), Center of Excellence in Materials Engineering (CEME), the Energy Technology Research Centre (ETRC), and the Graduate school scholarship from the Prince of Songkla University. The authors would also like to thank the Faculty of Engineering, Faculty of Environmental Management, Prince of Songkla University and Faculty of Applied Sciences, Universiti Teknologi MARA, Malaysia, for facility support.

REFERENCES CITED

- Araújo, A. J. M., Grilo, J. P.F., Loureiro, F. J. A., Campos, L. F. A., Paskocimas, C. A., Nascimento, R. M., and Macedo, D. A. (2018). "Designing experiments for the preparation of Ni-GDC cermet with controlled porosity as SOFC anode materials: Effects on the electrical properties," *Ceramics International* 44 (8), 23088-23093. DOI: 10.1016/j.ceramint.2018.09.115
- Ashok, J., Das, S., Dewangan, N., and Kawi, S. (2019). "H₂S and NO_x tolerance capability of CeO₂ doped La_{1-x}Ce_xCo_{0.5}Ti_{0.5}O_{3-δ} perovskites for steam reforming of biomass tar model reaction," *Energy Conversion and Management: X* 1, 100003. DOI: 10.1016/j.ecmx.2019.100003
- Amin, R., Chang, X., and Liu, B. (2017). "Synergistic effect of CeO₂ in CH₄/CO₂ Dry reforming reaction over stable xCeO₂ yNi/MCM-22 catalysts," *Industrial & Engineering Chemistry Research* 56 (26), 7445-7453. DOI: 10.1021/acs.iecr.7b01375
- Bao, C., Wang, Y., Feng, D., Jiang, Z., and Zhang, X. (2018). "Macroscopic modeling of solid oxide fuel cell (SOFC) and model-based control of SOFC and gas turbine hybrid system," *Progress in Energy and Combustion Science* 66, 83-140. DOI: 10.1016/j.peccs.2017.12.002
- Chea, S., Luengchavanon, M., Ananchaenwong, E., Techato, K., Jutidamrongphan, W., Chaiprapat, S., Niyomwas, S., and Marthosa, S. (2020). "Development of an O-ring from NR/EPDM filled silica/CB hybrid filler for use in a solid oxide fuel cell testing system," *Polymer Testing* 88, article no. 106568. DOI: 10.1016/j.polymertesting.2020.106568
- Chaiprapat, S., Wongchana, S., Loykulnant, S., Kongkaew, C., and Charnnok, B. (2015). "Evaluating sulfuric acid reduction, substitution, and recovery to improve environmental performance and biogas productivity in rubber latex industry," *Process Safety and Environmental Protection* 94, 420-429. DOI: 10.1016/j.psep.2014.10.002
- Charnnok, B., Suksaroj, T., Boonswang, P., and Chaiprapat, S. (2013). "Oxidation of hydrogen sulfide in biogas using dissolved oxygen in the extreme acidic biofiltration operation," *Bioresource Technology* 131, 492-499. DOI: 10.1016/j.biortech.2012.12.114
- Chen, R., Li, Z., Feng, J., Zhao, L., and Yu, J. (2020). "Effects of digestate recirculation ratios on biogas production and methane yield of continuous dry anaerobic digestion," *Bioresource Technology* 316, 123963. DOI: 10.1016/j.biortech.2020.123963
- Choolaei, M., Cai, Q., Slade, R.C.T., and Amini Horri, B. (2018). "Nanocrystalline gadolinium-doped ceria (GDC) for SOFCs by an environmentally-friendly single step method," *Ceramics International* 44 (11), 13286-13292. DOI:

- 10.1016/j.ceramint.2018.04.159
- Cruz, V. G. M., Costa, A. L. H., and Paredes, M. L. L. (2015). "Development and evaluation of a new DGA diagnostic method based on thermodynamics fundamentals," *IEEE Transactions on Dielectrics and Electrical Insulation* 22(2), 888-894. DOI: 10.1109/TDEI.2015.7076789
- Ding, C., Lin, H., Sato, K., and Hashida, T. (2009). "Synthesis of NiO–Ce_{0.9}Gd_{0.1}O_{1.95} nanocomposite powders for low-temperature solid oxide fuel cell anodes by co-precipitation," *Scripta Materialia* 60(4), 254-256. DOI: 10.1016/j.scriptamat.2008.10.020
- Fan, J., Wang, F., Sun, Q., Bin, F., Ding, J., and Ye, H. (2017). "SOFC detector for portable gas chromatography: High-sensitivity detection of dissolved gases in transformer oil," *IEEE Transactions on Dielectrics and Electrical Insulation* 24(5), 2854-2863. DOI: 10.1109/TDEI.2017.006438
- Guo, T., Zhang, L., Song, X., Dong, X., and Shirolkar, M. M., Wang, M., Li, M., and Wang, H. (2014). "Influences of Gd₂Ti₂O₇ sintering aid on the densification, ionic conductivity and thermal expansion of Gd_{0.1}Ce_{0.9}O_{1.95} electrolyte for solid oxide fuel cells," *Journal of Power Sources* 262, 239-244. DOI: 10.1016/J.JPOWSOUR.2014.03.077
- Gür, T. M. (2016). "Comprehensive review of methane conversion in solid oxide fuel cells: Prospects for efficient electricity generation from natural gas," *Progress in Energy and Combustion Science* 54, 1-64. DOI: 10.1016/j.peccs.2015.10.004
- Hing, P., Suklueng, M., Voo N. Y., Lim L. C., and Atkinson A. (2015). "Solid oxide fuel cells using novel cathodes in the BaO-Co₂O₃-Fe₂O₃ composited with GDC₁₀," *ECS Transactions* 68(1), 1837-1848. DOI: 10.1149/06801.1837ecst
- Hajakbari, F. (2020). "Characterization of nano crystalline nickel oxide thin films prepared at different thermal oxidation temperatures," *J. Nanostruct. Chem.* 10, 97-103. DOI: 10.1007/s40097-020-00332-2
- Irshad, M., Siraj, K., Raza, R., Javed, F., Ahsan, M., Shakir, I., and Rafique, M. S. (2016). "High performance of SDC and GDC core shell type composite electrolytes using methane as a fuel for low temperature SOFC," *AIP Advances* 6(2), article ID 025202. DOI: 10.1063/1.4941676
- Jadhav, S. T., Puri, V. R., and Jadhav, L. D. (2016). "NiO-GDC-BCY composites as an anode for SOFC," *Journal of Alloys and Compounds* 685, 626-632. DOI: 10.1016/j.jallcom.2016.05.243
- Jasinski, P., Suzuki, T., and Anderson, H. U. (2003). "Nanocrystalline undoped ceria oxygen sensor," *Sensors and Actuators B* 95, 73-77. DOI: 10.1016/S0925-4005(03)00407-6
- Kulkarni, S., Duttagupta, S., and Phatak, G. (2014). "Study of glycine nitrate precursor method for the synthesis of gadolinium doped ceria (Ce_{0.8}Gd_{0.2}O_{1.90}) as an electrolyte for intermediate temperature solid oxide fuel cells," *RSC Advances* 4, 46602-46612. DOI: 10.1039/C4RA06602B
- Kushi, T. (2016). "Performance and durability evaluation of dry reforming in solid oxide fuel cells," *International Journal of Hydrogen Energy* 41(39), 17567-17576. DOI: 10.1016/j.ijhydene.2016.07.025
- Kim, H., Kwon, J., Choi, S. Y., and Ahn, Y. G. (2019). "Method development for the quantitative determination of short chain fatty acids in microbial samples by solid phase extraction and gas chromatography with flame ionization detection," *Journal of Analytical Science and Technology* 10(28), 2-6. DOI: 10.1186/s40543-019-0184-2

- Lee, H.-C., Lee, J.-A., Lee, J.-H., Heo, Y.-W., and Kim, J.-J. (2017). "Ionic conductivity and relaxations of In-doped GDC (gadolinium doped ceria) ceramics," *Ceramics International* 43(15), 11792-11798. DOI: 10.1016/j.ceramint.2017.06.018
- Lengden, M., Cunningham, R., and Johnstone, W. (2013). "Tunable diode laser based concentration measurements of water vapour and methane on a solid oxide fuel cell," *Journal of Lightwave Technology* 31(9), 1354-1359. DOI: 10.1109/JLT.2013.2247378
- Liu, A. Z., Wang, J. X., He, C. R., Miao, H., Zhang, Y., and Wang, W. G. (2013). "Synthesis and characterization of Gd_{0.1}Ce_{0.9}O_{1.95} nanopowder via an acetic-acrylic method," *Ceramics International* 39(6), 6229-6235. DOI: 10.1016/j.ceramint.2013.01.044
- Malinga, N. N., and Jarvis, A. L. L. (2020). "Synthesis, characterization and magnetic properties of Ni, Co and FeCo nanoparticles on reduced graphene oxide for removal of Cr(VI)," *J. Nanostruct. Chem.* 10, 55-68. DOI: 10.1007/s40097-019-00328-7
- Mediseti, S., Ahn, J., Patil, S., Goel, A., Bangaru, Y., Sabhahit, G. V., Babu, G. U. B., Lee, J.-H., and Dasari, H. P. (2017). "Synthesis of GDC electrolyte material for IT-SOFCs using glucose & fructose and its characterization," *Nano-Structures & Nano-Objects* 11, 7-12. DOI: 10.1016/j.nanoso.2017.05.009
- Muñoz, F. F., Acuña, L. M., Albornoz, C. A., Leyva, A. G., Bakere, R. T., and Fuentes, R. O. (2015). "Redox properties of nanostructured lanthanide doped ceria spheres prepared by microwave assisted hydrothermal homogeneous co-precipitation," *Nanoscale* 7, 271-281. DOI: 10.1039/c4nr05630b
- Niaz, A.K., Jung, M.G., Park, J-Y., Anil V. Virkar, A.V. and Lim, H-T. (2019). "Spatial investigation of electronic properties in composite electrolytes for solid oxide fuel cells using embedded probes," *Journal of Power Sources* 438 (226945) 1-8. DOI: 10.1016/j.jpowsour.2019.226945
- Ohimain, E.I., Izah, S.C. (2017). "A review of biogas production from palm oil mill effluents using different configurations of bioreactors," *Renewable and Sustainable Energy Reviews* 70, 242-253. DOI: 10.1016/j.rser.2016.11.221
- Pan, Y.-X., Liu, C.-J., and Shi, P. (2008). "Preparation and characterization of coke resistant Ni/SiO₂ catalyst for carbon dioxide reforming of methane," *Journal of Power Sources* 176(1), 46-53. DOI: 10.1016/j.jpowsour.2007.10.039
- Paolini, V., Torre, M., Giacomini, W., Pastori, M., Segreto, M., Tomassetti, L., Carnevale, M., Gallucci, F., Petracchini, F., and Guerriero, E. (2019). "CO₂/CH₄ separation by hot potassium carbonate absorption for biogas upgrading," *International Journal of Greenhouse Gas Control* 83, 186-194. DOI: 10.1016/j.ijggc.2019.02.011
- Phaijit, S., Suklueng, M., Marthosa, S., Niyomwas, S., Voo, N. Y., and Kumar, A. (2019). "A novel micro-solid oxide fuel cell (μ -SOFC) for detecting methane content in biogas," *Bulletin of Materials Science* 42, 129. DOI: 10.1007/s12034-019-1789-1
- Rehman, S.u., Song, R.-H., Lee, J.-W., Lim, T.-H., Park, S.-J. Lee, S.-B. (2017). "Fabrication and characterization of La_{0.65}Sr_{0.3}MnO_{3- δ} /(Y₂O₃)_{0.08}(ZrO₂)_{0.92}/Gd_{0.1}Ce_{0.9}O_{2- δ} tri-composite cathode-supported tubular direct carbon solid oxide fuel cell," *Ceramics International* 43 (1 Part B), 1086-1091. DOI: 10.1016/j.ceramint.2016.10.045
- Rastrello, F., Placidi, P., Scorzoni, A., Cozzani, E., Messina, M., Elmi, I., Zampolli, S., and Cardinali, G. C. (2013). "Thermal conductivity detector for gas chromatography: Very wide gain range acquisition system and experimental measurements," *IEEE Transactions on Instrumentation and Measurement* 62(5), 974-981.

DOI: 10.1109/TIM.2012.2236723

- Rehman, S. U., Song, R.-H., Lee, J.-W., Lim, T.-H. Park, S.-J., and Lee, S.-B. (2016). "Effect of GDC addition method on the properties of LSM–YSZ composite cathode support for solid oxide fuel cells," *Ceramics International* 42(10), 11772-11779. DOI: 10.1016/j.ceramint.2016.04.098
- Suklueng, M., Yoong, V. N., Peter, H., and Ming, L. C. (2014). "Optimization of a novel composite cathode for intermediate temperature SOFCs applications," *Walailak Journal of Science and Technology (WJST)* 12(4), 373-381. DOI: 10.14456/WJST.2015.29
- Setevich, C. F., Mogni, L. V., Caneiro, A., and Prado, F. D. (2012). "Optimum cathode configuration for IT-SOFC using $\text{La}_{0.4}\text{Ba}_{0.6}\text{CoO}_{3-\delta}$ and $\text{Ce}_{0.9}\text{Gd}_{0.1}\text{O}_{1.95}$," *International Journal of Hydrogen Energy* 37(19), 14895-14901. DOI: 10.1016/j.ijhydene.2012.01.155
- Serret, P., Colominas, S., Reyes, G., and Abellà, J. (2011). "Characterization of ceramic materials for electrochemical hydrogen sensors," *Fusion Engineering and Design* 86(9-11), 2446-2449. DOI: 10.1016/j.fusengdes.2011.01.029
- Santos, H. A, J. A. F., and Matencio, R. Z. T. (2011). "Ceramic materials for solid oxide fuel cells, advances in ceramics - Synthesis and characterization," *Processing and Specific Applications-IntechOpen* 424-446. DOI: 10.5772/18297
- Thiabdokmai, C., Tangtrakarn, A., Promsuy, S., Ngiewlay, P., and Mongkolkachit, C. (2014). "Templateless synthesis and characterization of hollow gadolinium doped cerium oxide nanofibers by electrospinning," *Advances in Materials Science and Engineering* article no. 127531, 1-10. DOI: 10.1155/2014/127531
- Tian, W., Ho, Y., and Chou, C. (2013). "Photoactivated TiO_2 Gas chromatograph detector for diverse chemical compounds sensing at room temperature," *IEEE Sensors Journal* 13 (5), 1725-1729. DOI: 10.1109/JSEN.2013.2242259
- Wei, T., Jia, L., Zheng, H., Chi, B., Pu, J., and Li, J. (2018). "LaMnO₃-based perovskite with in-situ exsolved Ni nanoparticles: A highly active, performance stable and coking resistant catalyst for CO₂ dry reforming of CH₄," *Applied Catalysis A: General* 564, 199-207. DOI: 10.1016/j.apcata.2018.07.031
- Xia, C., Chen, F., and Liu, M. (2001). "Reduced-temperature solid oxide fuel cells fabricated by screen printing," *Electrochemical and Solid-State Letters* 4(5), A52-A54. DOI: 10.1149/1.1361158

Article submitted: June 24, 2021; Peer review completed: October 30, 2021; Revised version received and accepted: November 11, 2021; Published: November 17, 2021. DOI: 10.15376/biores.17.1.281-298